

Digital Predistortion of Power Amplifiers for Wireless Applications

A Thesis
Presented to
The Academic Faculty

by

Lei Ding

In Partial Fulfillment
of the Requirements for the Degree
Doctor of Philosophy

School of Electrical and Computer Engineering
Georgia Institute of Technology
March 2004

UMI Number: 3126235

PREVIEW

UMI[®]

UMI Microform 3126235

Copyright 2004 by ProQuest Information and Learning Company.

All rights reserved. This microform edition is protected against
unauthorized copying under Title 17, United States Code.

ProQuest Information and Learning Company
300 North Zeeb Road
PO Box 1346
Ann Arbor, MI 48106-1346

Digital Predistortion of Power Amplifiers for Wireless Applications

Approved by:

Dr. G. Tong Zhou, Advisor

Dr. Ye (Geoffrey) Li

Dr. J. Stevenson Kenney

Dr. Jianmin Qu

Dr. W. Marshall Leach

Date Approved: April 1, 2004

PREVIEW

For my family.

ACKNOWLEDGEMENTS

It is time to draw a period to my PhD endeavor. I feel extremely lucky to meet so many talented people during these years. I am grateful for their friendship, help, encouragement, and support.

First, I would like to thank my advisor, Dr. G. Tong Zhou, for providing this opportunity for me to study at Georgia Tech. Her constant encouragement and valuable advices are essential for the completion of this thesis. I will be always inspired by the high standards she sets for herself and her sharp focus and deep devotion to whatever she works on.

I would like to thank my thesis committee members: Drs. J. Stevenson Kenney, W. Marshall Leach, Ye (Geoffrey) Li, and Jianmin Qu for taking time to serve on my committee and for their questions and suggestions. My special thanks also go to Drs. Monson Hayes and Douglas B. Williams for the excellent classes they offered, which benefit me a lot for my research work and job search.

I also benefit a lot from my two summer internships at Bell Labs, Lucent Technologies. I would like to thank Drs. Zhengxiang Ma and Dennis R. Morgan for making this possible. I enjoyed every aspect of my internship experience: talented colleagues, excellent research opportunities, cool weather, nice work environment, and the list goes on. My special thanks also go to Dr. Yiteng Huang for his friendship and help during my stay in New Jersey.

I would like to thank my group members: Yongsub, Krishna, Muhammad, Raviv, Gail, Ning, Hua, Chunpeng, Yuan, Thao, Vincent, and Bob for all the technical discussions and help along the way. I also enjoyed interactions with the nice Chinese student community here at CSIP.

A lot of credit goes to my parents. Their unconditional support has always helped me in all my endeavors. I would also like to thank my sister for her support and feeding me with great dishes from time to time. Last but not least, I would like to thank my wife, wenjin, for her love, encouragement, and support.

TABLE OF CONTENTS

Dedication	iii
Acknowledgements	iv
List of Tables	viii
List of Figures	ix
Summary	xiii
Chapter 1 Introduction	1
1.1 Motivation	1
1.2 Objectives	3
1.3 Outline	3
Chapter 2 Background	5
2.1 Modeling Memoryless Power Amplifiers	5
2.2 Predistortion of Memoryless Power Amplifier	7
2.2.1 Data Predistortion for Memoryless Power Amplifiers	7
2.2.2 Signal Predistortion for Memoryless Power Amplifiers	8
2.3 Modeling Power Amplifiers with Memory Effects	10
2.4 Predistortion of Power Amplifiers with Memory Effects	14
Chapter 3 Digital Predistorter Design	17
3.1 Hammerstein Predistorter Design	17
3.1.1 Hammerstein Predistorter Training	17
3.1.2 Hammerstein Predistorter Simulation	22
3.2 Memory Polynomial Predistorter Design	25
3.2.1 Memory Polynomial Predistorter Training	25
3.2.2 Memory Polynomial Predistorter Simulation	26
3.2.3 Memory Polynomial Predistorter Discussion	33
3.3 A New Combined Predistorter Design	35
3.3.1 Combined Predistorter Model	36
3.3.2 Combined Predistorter Training	37
3.3.3 Effects of Noise and Initial Estimates	40

3.3.4	Combined Predistorter Performance	45
Chapter 4	Effects of Even-order Nonlinear Terms	47
4.1	Passband and Baseband Nonlinearities	47
4.1.1	Memoryless Case	47
4.1.2	Quasi-memoryless Case	48
4.2	Even-Order Terms in the Baseband Power Amplifier Model	50
4.3	Even-Order Terms in the Baseband Predistorter Model	53
4.4	Extensions to Power Amplifiers and Predistorters with Memory	58
Chapter 5	Analog Imperfection Compensation	61
5.1	Two-Stage Upconversion Transmitter	61
5.1.1	System Setup	61
5.1.2	Channel Estimation	62
5.1.3	Equalizer Design	65
5.1.4	Experimental Results	67
5.2	Direct Upconversion Transmitter	71
5.2.1	Channel Models	72
5.2.2	Channel Estimation	76
5.2.3	Compensator Construction	79
5.2.4	Simulations	84
Chapter 6	Real-time Implementations	87
6.1	Memory Polynomial Model	87
6.2	Indirect Learning Architecture	88
6.3	Predistorter Construction	88
6.4	DSP Implementation	91
6.4.1	Implementation Details	91
6.4.2	Performance Evaluation	92
6.5	Testbed Measurements	92
Chapter 7	Conclusions	98
7.1	Contributions	98
7.2	Suggestions for Future Research	99

References	100
----------------------	-----

PREVIEW

LIST OF TABLES

Table 1	NMSE for $F(z(t))$	52
Table 2	NMSE for $G(x(t))$	55
Table 3	NMSE when the power amplifier is modeled by memory polynomial. . . .	58
Table 4	Ideal Model Coefficients	84
Table 5	Real-time performance of the predistorter training algorithm.	94

PREVIEW

LIST OF FIGURES

Figure 1	Digital Predistortion System Diagram	2
Figure 2	The AM/AM and AM/PM responses of a Class AB power amplifier. . . .	6
Figure 3	Block diagram of a data predistortion system with the pulse shaping filter implemented after the power amplifier.	7
Figure 4	Block diagram of a data predistortion system with the pulse shaping filter placed in the baseband after the predistorter.	8
Figure 5	Block diagram of a signal predistortion system.	9
Figure 6	The Wiener Model.	12
Figure 7	The Hammerstein Model.	12
Figure 8	The Wiener-Hammerstein model.	12
Figure 9	The indirect learning architecture for the predistorter.	15
Figure 10	The indirect learning architecture for the Hammerstein predistorter. . . .	18
Figure 11	Comparison of the PSDs for the pole/zero Wiener power amplifier and the pole/zero Hammerstein predistorter. (a) Output without predistortion; (b) Output with memoryless predistortion; (c) Output with Hammerstein predistortion, NG and LS/SVD algorithms (similar performance).	23
Figure 12	Comparison of the PSDs for FIR Wiener power amplifier and 15-tap FIR Hammerstein predistorter. (a) Output without predistortion; (b) Output with memoryless predistortion; (c) Output with Hammerstein predistortion (NG); (d) Output with Hammerstein predistortion (LS/SVD). . . .	24
Figure 13	Comparison of the PSDs for full Volterra power amplifier and 15-tap FIR Hammerstein predistorter. (a) Output without predistortion; (b) Output with memoryless predistortion; (c) Output with Hammerstein predistortion (NG); (d) Output with Hammerstein predistortion (LS/SVD); (e) Input signal.	24
Figure 14	The indirect learning architecture for the memory polynomial predistorter. . . .	26
Figure 15	Wiener-Hammerstein model diagram.	27
Figure 16	Effectiveness of predistortion in suppressing spectral regrowth when the power amplifier is modeled by a Wiener-Hammerstein system. (a) Output without predistortion; (b) Output with memoryless predistortion; (c) Output with memory polynomial predistortion ($Q = 2, K = 5$) (d) Original input. (c) and (d) almost coincide.	28

Figure 17	Effectiveness of predistortion in suppressing spectral regrowth, when the power amplifier itself is modeled by a memory polynomial. (a) Output without predistortion; (b) Output with memoryless predistortion; (c) Output with memory polynomial predistortion ($Q = 2, K = 5$, odd order); (d) Output with memory polynomial predistortion ($Q = 2, K = 5$, even and odd orders); (e) Original input.	29
Figure 18	Effectiveness of predistortion in suppressing spectral regrowth, when the power amplifier is modeled by a perturbed Wiener (hence Volterra) system. (a) Output without predistortion; (b) Output with memoryless predistortion; (c) Output with memory polynomial predistortion ($Q = 2, K = 5$); (d) Output with memory polynomial predistortion ($Q = 10, K = 5$); (e) Original input.	29
Figure 19	Parallel Wiener model diagram. $H_i(\cdot)$ is an LTI block, and $F_i(\cdot)$ is a memoryless nonlinear block.	32
Figure 20	Effectiveness of predistortion in suppressing spectral regrowth, when the power amplifier is modeled by a parallel Wiener system. (a) Output without predistortion; (b) Output with memoryless predistortion; (c) Output with memory polynomial predistortion ($Q = 2, K = 5$); (d) Output with memory polynomial predistortion ($Q = 5, K = 5$); (e) Original input. . .	32
Figure 21	Parallel Hammerstein model diagram. $F_i(\cdot)$ is a memoryless nonlinear block, and $H_i(\cdot)$ is an LTI block.	34
Figure 22	The indirect learning architecture of the new combined predistorter model.	37
Figure 23	Block diagram of the predistorter model simulation.	41
Figure 24	Trajectories of (a) mean squared error, (b) c_l coefficients, (c) amplitudes of a_{kp} coefficients, and (d) amplitudes of b_q coefficients vs. number of iterations in the noiseless setting.	43
Figure 25	Trajectories of (a) mean squared error, (b) c_l coefficients, (c) amplitudes of a_{kp} coefficients, and (d) amplitudes of b_q coefficients vs. number of iterations in the noisy setting.	43
Figure 26	Comparison of the power spectrum of the noiseless predistorter model output $z_0(n)$ with the power spectra of noiseless residue $e_0(n)$ in noiseless and noisy settings.	44
Figure 27	Comparison of the power spectrum of the noiseless predistorter model output $z_0(n)$ with the power spectra of noiseless residue $e_0(n)$ for different initialization \mathbf{c} 's in the noisy setting.	44
Figure 28	Overall system performance of the least-squares/Newton algorithm on the predistortion testbed, showing the power spectra of the output signal (a) without predistortion, (b) with predistorter ($\mathbf{m} = [7 \ 4 \ 0 \ 0]$), (c) with predistorter ($\mathbf{m} = [7 \ 4 \ 7 \ 3]$), and (d) with predistorter ($\mathbf{m} = [7 \ 4 \ 7 \ 35]$).	46

Figure 29	Fitting $F(z(t))$ using polynomials of different orders. (a) and (b) show the real and imaginary parts of the measured $F(z(t))$ and its polynomial approximations $\hat{F}(z(t))$. (c) and (d) show the real and imaginary parts of the fitting error $\hat{F}(z(t)) - F(z(t))$. In all figures, LUT refers to the measured power amplifier data, and the polynomial order sets $\mathcal{K}_1 = \{1, 3, 5\}$, $\mathcal{K}_2 = \{1, 3, 5, 7, 9\}$, $\mathcal{K}_3 = \{1, 2, 3, 4, 5\}$	52
Figure 30	The predistorter precedes the power amplifier, and the objective is to have $y(t) \approx Cx(t)$, where C is a constant.	53
Figure 31	The errors $\hat{G}(x(t)) - G(x(t))$ for three sets of polynomial orders $\mathcal{L}_1 = \{1, 3, 5, 7\}$, $\mathcal{L}_2 = \{1, 3, 5, 7, 9, 11, 13\}$, and $\mathcal{L}_3 = \{1, 2, 3, 4, 5, 6, 7\}$. The real part of the error is shown in Figure (a), and the imaginary part of the error is shown in Figure (b). \mathcal{L}_2 and \mathcal{L}_3 resulted in comparable amount of error and both outperform \mathcal{L}_1	56
Figure 32	Predistortion linearization performance in terms of spectral regrowth suppression. power amplifier output power spectral density (PSD) is shown for the following cases: (a) there is no predistorter; (b) predistorter (119) with $\mathcal{L}_1 = \{1, 3, 5, 7\}$ is used; (c) predistorter (119) with $\mathcal{L}_2 = \{1, 3, 5, 7, 9, 11, 13\}$ or predistorter (119) with $\mathcal{L}_3 = \{1, 2, 3, 4, 5, 6, 7\}$ is used (the two lines coincide). (d) PSD of the original input.	57
Figure 33	Predistortion linearization performance in terms of spectral regrowth suppression. Power amplifier output power spectral density (PSD) is shown for the following cases: (a) there is no predistorter; (b) predistorter (123) with $\mathcal{L}_1 = \{1, 3, 5, 7\}$ and $Q = 4$ is used; (c) predistorter (123) with $\mathcal{L}_2 = \{1, 3, 5, 7, 9, 11, 13\}$ and $Q = 4$ is used; (d) predistorter (123) with $\mathcal{L}_3 = \{1, 2, 3, 4, 5, 6, 7\}$ and $Q = 4$ is used. (e) PSD of the original input.	60
Figure 34	Two-stage upconversion transmitter.	62
Figure 35	Block diagram of the baseband predistortion system with equalization. The dashed lines refer to the feedback path for equalizer training.	62
Figure 36	Comparison between noncausal system response $H(e^{j\omega})$ (solid line) and causal system response $H_c(e^{j\omega})$ (dotted-line). Note that the mean slopes of the phase responses have been removed. The phase responses of $H(e^{j\omega})$ and $H_c(e^{j\omega})$ coincide.	65
Figure 37	Block diagram of the test bed.	68
Figure 38	Example of a training signal from predistorted waveform with the equalizer turned off.	69
Figure 39	Magnitude and phase responses of the estimated channel (solid line), the equalizer (dotted line), and the overall cascade of the channel and the equalizer (dashed line). The estimated channel has 51 taps. The equalizer has 14 taps and is designed with $\omega_p = 0.7\pi$, $w = 10^{-3}$	69

Figure 40	Comparison of power spectral densities (PSDs). (a) Training signal; (b) Power Amplifier output with predistortion but no equalizer; (c) PA output with predistortion and equalizer; (d) PA output with the same predistorter as in (c) but no equalizer.	70
Figure 41	Block diagram of the baseband predistortion system. The dashed lines refer to the feedback loop for I/Q compensator training.	73
Figure 42	Detailed block diagram of the path from the DAC input $x(n)$ to the baseband feedback data samples $y(n)$	73
Figure 43	Block diagrams of three channel models: (a) real I/Q model; (b) complex I/Q model; (c) direct/image model.	74
Figure 44	Cascade of the I/Q compensator and the channel.	79
Figure 45	Comparison of the direct upconverter outputs without I/Q compensation and with different I/Q compensators. (a) Without I/Q compensation; (b) With a 1-tap I/Q compensator; (c) With a 9/9 I/Q compensator constructed using the two-step approach; (d) With a 9-tap I/Q compensator constructed using the one-step approach; (e) Original input. Here, (c), (d), and (e) coincide.	85
Figure 46	Comparison of the power amplifier output with different I/Q compensators and predistorters. (a) Without predistortion but with a 9-tap I/Q compensation from the one-step approach; (b) With predistortion and a 1-tap I/Q compensator; (c) With predistortion and a 9/9 I/Q compensator from the two-step approach; (d) With predistortion and a 9-tap I/Q compensator from the one-step approach; (e) Original input. Here, (c), (d), and (e) almost coincide.	86
Figure 47	The indirect learning architecture for the predistorter.	88
Figure 48	Condition number of the correlation matrix with different Q values and different input signals: (a) three-carrier WCDMA with $K = 5$ conventional polynomials; (b) three-carrier WCDMA with $K = 5$ orthogonal polynomials; (c) a complex random signal (amplitude uniformly distributed in $[0,1]$) with $K = 5$ conventional polynomials; (d) a complex random signal (amplitude uniformly distributed in $[0,1]$) with $K = 5$ orthogonal polynomials.	91
Figure 49	Flow chart of the algorithm.	93
Figure 50	Block diagram of the testbed.	94
Figure 51	Measured power amplifier output PSD: (a) without predistortion; (b) with $K = 5$ memoryless predistorter trained by 5,000 data samples; (c) with $K = 5$ memoryless predistorter trained by 20,000 data samples. (b) and (c) coincide.	96
Figure 52	Measured power amplifier output PSD: (a) without predistortion; (b) with $K = 5$, $Q = 4$ memory polynomial predistorter trained by 5,000 data samples; (c) with $K = 5$, $Q = 4$ memory polynomial predistorter trained by 20,000 data samples.	97

SUMMARY

Power amplifiers are essential components in communication systems and are inherently nonlinear. The nonlinearity creates spectral growth (broadening) beyond the signal bandwidth, which interferes with adjacent channels. It also causes distortions within the signal bandwidth, which decreases the bit error rate at the receiver. Newer transmission formats, such as wideband code division multiple access (WCDMA) or orthogonal frequency division multiplexing (OFDM), are especially vulnerable to the nonlinear distortions due to their high peak-to-average power ratios (PAPRs). If we simply back-off the input signal to achieve the linearity required for the power amplifier, the power amplifier efficiency will be very low for high PAPR signals.

Another choice is to linearize a nonlinear power amplifier so that overall we have a linear and reasonably efficient device. Digital predistortion is one of the most cost effective ways among all linearization techniques. However, most of the existing designs treat the power amplifier as a memoryless device. For wideband or high power applications, the power amplifier exhibits memory effects, for which memoryless predistorters can achieve only limited linearization performance.

In this dissertation, we propose novel predistorters and their parameter extraction algorithms. We investigate a Hammerstein predistorter, a memory polynomial predistorter, and a new combined model based predistorter. The Hammerstein predistorter is designed specifically for power amplifiers that can be modeled as a Wiener system. The memory polynomial predistorter can correct both the nonlinear distortions and the linear frequency response that may exist in the power amplifier. It is a robust predistorter, which has demonstrated good performance on several nonlinear system models. Real-time implementation aspects of the memory polynomial predistorter are also investigated in the dissertation. The new combined model includes the memory polynomial model and the Murray Hill model, thus extending the predistorter's ability to compensate for strong memory effects in

the power amplifier. Performance of the new model is demonstrated through experimental measurements.

The predistorter models considered in this dissertation include both even- and odd-order nonlinear terms. In the literature, most of the power amplifier and predistorter models consider only the odd-order terms. Here, we show that it is beneficial to include even-order nonlinear terms in both the baseband power amplifier and predistorter models. By including these even-order nonlinear terms, we have a richer basis set, which offers appreciable improvement.

The ideal performance of digital predistortion certainly relies on robust predistorters that can completely compensate for the nonlinearities of the power amplifier. In reality, however, the performance can also be affected by the analog imperfections in the transmitter, which are introduced by the analog components; mostly analog filters and quadrature modulators. There are two common configurations for the upconversion chain in the transmitter: two-stage upconversion and direct upconversion. For a two-stage upconversion transmitter, we design a band-limited equalizer to compensate for the frequency response of the surface acoustic wave (SAW) filter which is usually employed in the IF stage. For a direct upconversion transmitter, we develop a model to describe the frequency-dependent gain/phase imbalance and dc offset. We then develop two methods to construct compensators for the imbalance and dc offset. These compensation techniques help to correct for the analog imperfections, which in turn improve the overall predistortion performance.

CHAPTER 1

INTRODUCTION

1.1 Motivation

Power amplifiers are indispensable components in a communication system and are inherently nonlinear. The nonlinearity generates spectral regrowth, which leads to adjacent channel interference and violations of the out-of-band emission requirements mandated by regulatory bodies. It also causes in-band distortion, which degrades the bit error rate (BER) performance.

To reduce the nonlinearity, the power amplifier can be backed off to operate within the linear portion of its operating curve. However, newer transmission formats, such as wideband code division multiple access (WCDMA) and orthogonal frequency division multiplexing (OFDM), have high peak to average power ratios, i.e., large fluctuations in their signal envelopes. This means that the power amplifier needs to be backed off far from its saturation point, which results in very low efficiencies, typically less than 10% [50]; i.e., more than 90% of the dc power is lost and turns into heat. Considering the large number of wireless base stations deployed worldwide, improved power amplifier efficiency can substantially reduce the electricity and cooling costs incurred to the service providers. To improve the power amplifier efficiency without compromising its linearity, power amplifier linearization is essential.

Among all linearization techniques, digital predistortion is one of the most cost effective (see Fig. 1). It adds a digital predistorter in the baseband to create an expanding nonlinearity that is complementary to the compressing characteristic of the power amplifier. Ideally, the cascade of the predistorter and the power amplifier becomes linear and the original input is amplified by a constant gain. With the predistorter, the power amplifier can be utilized up to its saturation point while still maintaining a good linearity, thereby significantly increasing its efficiency. In reality, the power amplifier characteristics may change

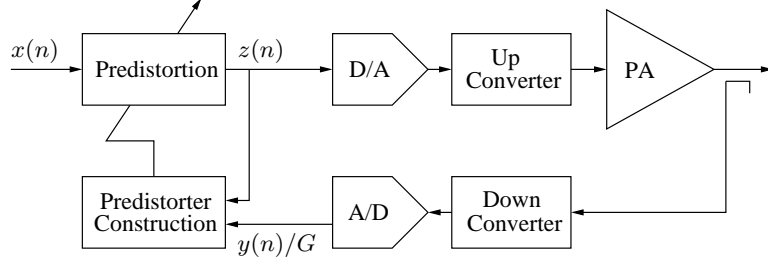


Figure 1: Digital Predistortion System Diagram

over time because of temperature drift, component aging, etc. Therefore, the predistorter should also have the ability to adapt to these changes.

Digital predistortion implementations in the current literature mostly focus on the power amplifier that has a memoryless nonlinearity; i.e., the current output depends only on the current input through a nonlinear mechanism. This instantaneous nonlinearity is usually characterized by the AM/AM and AM/PM responses of the power amplifier, where the output signal amplitude and phase deviation of the power amplifier output are given as functions of the amplitude of its current input. There has been intensive research on predistortion techniques for memoryless power amplifiers during the past decade [28].

As the signal bandwidth gets wider, such as in WCDMA, power amplifiers begin to exhibit memory effects. This is especially true for those high power amplifiers used in wireless base stations. The causes of the memory effects can be attributed to thermal constants of the active devices or components in the biasing network that have frequency-dependent behaviors [47]. As a result, the current output of the power amplifier depends not only on the current input, but also on past input values. In other words, the power amplifier becomes a nonlinear system with memory. For such a power amplifier, memoryless predistortion can achieve only very limited linearization performance [29], [17]. Therefore, digital predistorters also need to have memory structures. This dissertation investigates robust predistorter models that are capable of linearizing power amplifiers with memory effects. It also investigates system implementation issues related to these wideband digital predistortion systems.

1.2 Objectives

The objective of this dissertation is to develop digital predistortion systems for linearization of power amplifiers with memory effects. Our research efforts focus on three areas:

- Predistorter models with memory structures;
- Digital compensation techniques of analog imperfections in the transmitters;
- Wideband digital predistortion testbed.

Volterra series is a general nonlinear model with memory. However, the large number of coefficients in the Volterra series makes it unattractive for practical applications. Instead, several special cases of the Volterra series are considered in this dissertation, which include the Hammerstein model [25], the memory polynomial model [30], the Murray Hill model [32], and possible combinations of these models.

The ideal performance of digital predistortion certainly relies on robust predistorters that can completely compensate for the nonlinearities in the power amplifier. In reality, however, the performance can also be affected by the analog imperfections in the transmitter, which are introduced by the analog components, such as mixers, analog filters, and quadrature modulators. The second focus of this dissertation is to investigate modeling and compensation techniques for these imperfections.

In this dissertation, a wideband digital predistortion testbed is also developed to evaluate the performance of digital predistortion systems on real power amplifiers.

1.3 Outline

The dissertation is organized as follows:

Chapter 2 reviews the literature in the field of modeling and predistortion of power amplifiers. A memoryless power amplifier can be characterized by its AM/AM and AM/PM responses. To linearize such a power amplifier, a memoryless predistorter is sufficient. For a power amplifier with memory effects, various models are available to capture the behavior of the power amplifier, which include the Volterra series, the Wiener model, the Hammerstein

model, and the Wiener-Hammerstein model. The indirect learning architecture is then presented to construct the predistorter for a power amplifier with memory effects.

In Chapter 3, we present novel predistorters and their parameter extraction algorithms. A Hammerstein predistorter, a memory polynomial predistorter, and a new combined model based predistorter are considered. The parameters of these predistorters are extracted using the indirect learning architecture, eliminating the need for model assumption and parameter extraction of the power amplifier. Performance of these predistorters are demonstrated through computer simulations and/or experimental measurements.

Most existing literature considers only odd-order nonlinear terms when modeling power amplifiers and designing predistorters in the baseband. We show in Chapter 4 that it is beneficial to include even-order nonlinear terms in the baseband PA as well as predistorter models. By including these even-order nonlinear terms, we have a richer basis set, which offers appreciable improvement.

In Chapter 5, we study the analog imperfections in the transmitter and design compensation techniques. For a two-stage upconversion transmitter, we design a band-limited equalizer to compensate for the frequency response of the SAW filter, which is usually employed in the IF stage. For a direct upconversion transmitter, we develop a model to describe the frequency-dependent gain/phase imbalance and dc offset. We then develop two methods to construct compensators for the imbalance and dc offset. These compensation techniques help to correct for the analog imperfections, which in turn improve the overall predistortion performance.

In a practical implementation, predistorter training is performed on a digital signal processor, such as the Texas Instruments TMS320C6711. In Chapter 6, we investigate real-time implementation aspects of the memory polynomial predistorter. We implement the predistorter training algorithm on a Texas Instruments TMS320C6711 processor and evaluate the performance of the trained predistorter on our wideband digital predistortion testbed.

Finally, Chapter 7 concludes the dissertation and provides future research directions.

CHAPTER 2

BACKGROUND

In this chapter, we review modeling techniques and predistorter design for memoryless power amplifiers, as well as power amplifiers with memory effects.

2.1 Modeling Memoryless Power Amplifiers

In the passband, a strictly memoryless power amplifier can be described as a nonlinear function that maps a real valued input to a real valued output. Over a closed interval for $\tilde{z}(t)$, this memoryless nonlinearity can be approximated by a power series; i.e.,

$$\tilde{y}(t) = \sum_{k=1}^K \tilde{b}_k \tilde{z}^k(t), \quad (1)$$

where \tilde{b}_k are real-valued coefficients, $\tilde{z}(t)$ is the passband power amplifier input, and $\tilde{y}(t)$ is the passband power amplifier output. In the baseband, (1) becomes

$$y(t) = \sum_{\substack{k=1 \\ k \text{ odd}}}^K b_k z(t) |z(t)|^{k-1} \quad (2)$$

[3, p. 69], [39], where

$$b_k = 2^{1-k} \binom{k}{\frac{k-1}{2}} \tilde{b}_k, \quad (3)$$

$z(t)$ is the baseband power amplifier input, and $y(t)$ is the baseband power amplifier output. The first observation from (2) is that it only contains odd order terms. This is because the signals generated from the even order terms in (1) are far from the carrier frequency. Thus, they do not contribute to the baseband output $y(t)$. The second observation is that b_k are real valued since \tilde{b}_k are real valued. Therefore, if the power amplifier is strictly memoryless, it only introduces amplitude distortion to the input signal, giving rise to the so called AM/AM conversion of the power amplifier.

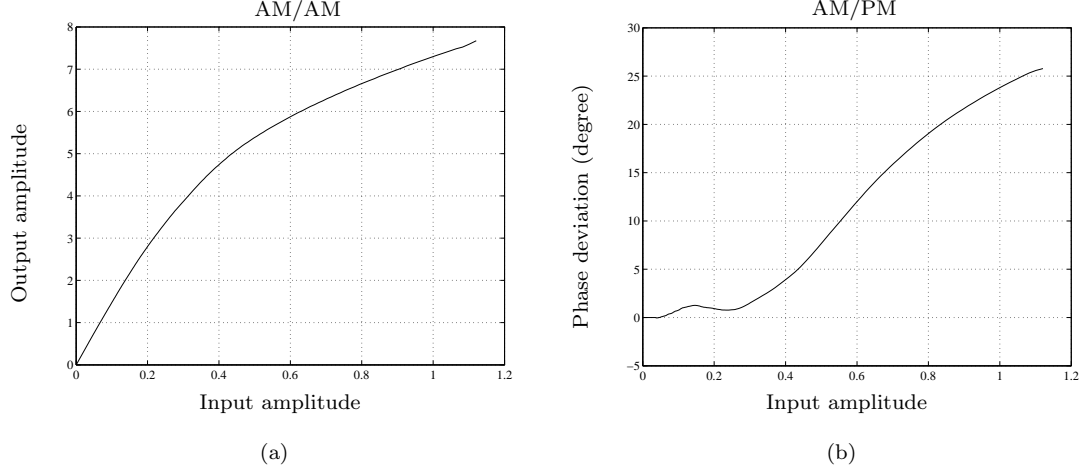


Figure 2: The AM/AM and AM/PM responses of a Class AB power amplifier.

Interestingly, if b_k in (2) are allowed to be complex, (2) can represent a much larger class of power amplifiers, often referred to as quasi-memoryless power amplifiers. In the passband, a nonlinear power amplifier with memory can be approximated by the Volterra series; i.e.,

$$\tilde{y}(t) = \sum_k \int \cdots \int \tilde{h}_k(\boldsymbol{\tau}_k) \prod_{i=1}^k \tilde{z}(t - \tau_i) d\boldsymbol{\tau}_k, \quad (4)$$

where $\boldsymbol{\tau}_k = [\tau_1, \dots, \tau_k]^T$, $\tilde{h}_k(\cdot)$ is the real-valued k th-order Volterra kernel, and $d\boldsymbol{\tau}_k = d\tau_1 d\tau_2 \cdots d\tau_k$. An important special case here is when the power amplifier in the passband has short-term memory; i.e., the time span of the memory is short compared to the time variations of the input signal envelope. With this assumption, it is shown in [39] that the baseband version of (4) has the same form as (2) except that b_k are complex valued. In this case, besides amplitude distortion, the power amplifier also introduces phase distortion to the input signal, which leads to the nonconstant AM/PM conversion of the power amplifier. However, the baseband representation in this case is still memoryless.

In summary, power amplifiers that are strictly memoryless or quasi-memoryless can be characterized by their AM/AM and AM/PM conversions. As an example, the AM/AM and AM/PM responses of a memoryless Class AB power amplifier are shown in Fig. 2.

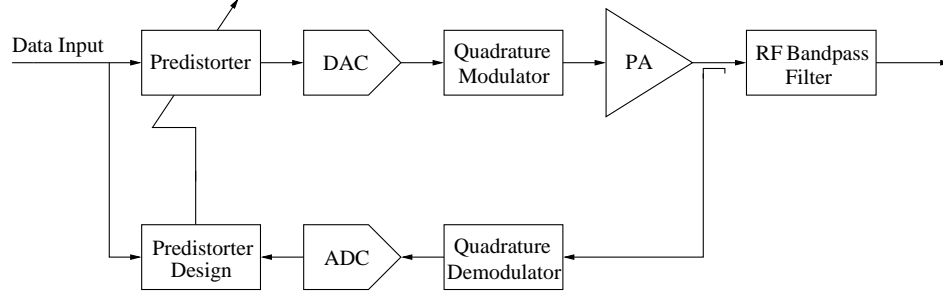


Figure 3: Block diagram of a data predistortion system with the pulse shaping filter implemented after the power amplifier.

2.2 *Predistortion of Memoryless Power Amplifier*

In the current literature, digital predistortion implementations mostly focus on memoryless power amplifiers.

2.2.1 Data Predistortion for Memoryless Power Amplifiers

Early digital predistorters mainly fall into the data predistorter category in the sense that predistortion is applied directly to each of the input signal constellation points. Depending on the location of the pulse shaping filter in the transmitter, there are two types of data predistorters.

The first type, exemplified by [24], [41], implements the pulse shaping filter using a radio frequency (RF) bandpass filter after the power amplifier. The schematic diagram of this type of predistortion system is shown in Fig. 3. Since the power amplifier is memoryless and there is no filtering between the predistorter and the power amplifier, it is sufficient to use a memoryless data predistorter here. The predistorter can be easily implemented as look-up tables (LUTs) that map the original input constellation points to the desired locations. Because of the small size of the input levels, this type of predistorters converges fast and requires very little memory. However, RF bandpass filters with sharp cut-offs are difficult to obtain and have relative large losses, thereby making this structure unattractive.

The second type, exemplified by [26], [27], [20], considers the case where the pulse shaping filter is placed in the baseband, immediately after the data predistorter (see Fig. 4). In such an arrangement, a memoryless data predistorter is not sufficient to fully linearize

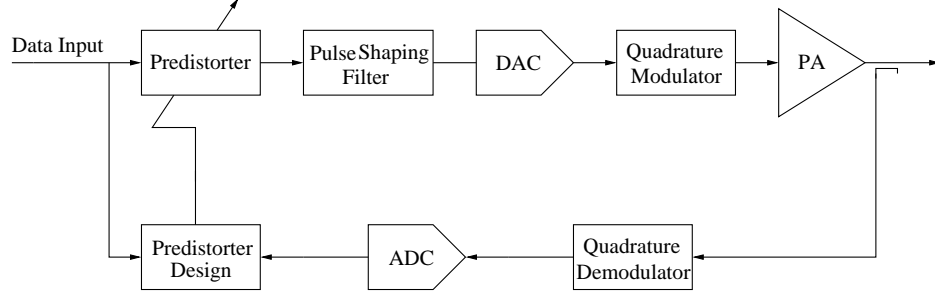


Figure 4: Block diagram of a data predistortion system with the pulse shaping filter placed in the baseband after the predistorter.

the memoryless power amplifier since it compensates only for those signal levels appearing in the signal constellation. The approach taken by [26] uses a specific pulse shaping filter to generate discrete values at two or three equally spaced data points per symbol interval. Each data point is then predistorted by a memoryless predistorter and combined with adjacent data points to reduce the nonlinear distortion at the power amplifier output. In [27], the current data input is considered together with its previous and following inputs as a signal point of a larger signal constellation, which is then predistorted by a memoryless data predistorter. Eun and Powers [20] proposed a Volterra series based data predistorter to compensate for the cascade of the pulse shaping filter and the power amplifier. The predistorter is trained using the indirect learning architecture, where the desired power amplifier output is set to be the original data after pulse shaping.

The main drawback of data predistorters is their dependence on the signal constellation and the pulse shaping filter. Moreover, data predistorters do not work well if the processing produces almost continuous input signal levels, e.g., in OFDM or WCDMA.

2.2.2 Signal Predistortion for Memoryless Power Amplifiers

To overcome these limitations, recent digital predistorters have usually been applied at the last stage of the baseband processing (see Fig. 5). In contrast to data predistorters, these predistorters can deal with arbitrary input waveforms, thus they are referred to as signal predistorters here. They can be divided into three categories [44]: mapping structure, polar structure, and complex gain structure.

The first signal predistorter for memoryless power amplifiers was proposed by Nagata

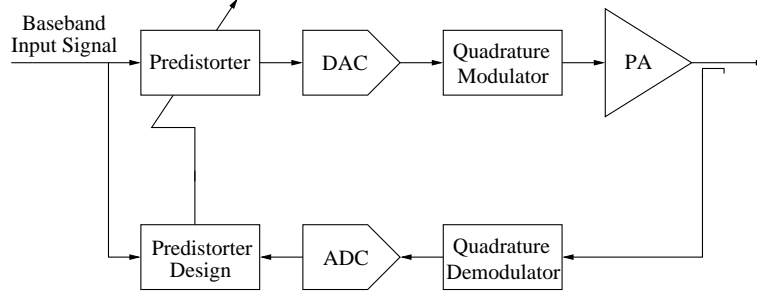


Figure 5: Block diagram of a signal predistortion system.

[36] using a mapping structure. Given a complex baseband input signal $x(t)$, the predistorter generates a complex correction signal $\Delta[x(t)]$ from a two-dimensional LUT indexed by the real and imaginary parts of $x(t)$. The predistorted signal $z(t)$ is given by

$$z(t) = x(t) + \Delta[x(t)]. \quad (5)$$

Thus, the predistorter maps each complex input point to its desired location, which is a generalization of the first type of data predistorters in Section 2.2.1. This nonlinear mapping can also correct for other types of memoryless distortions in the transmitter, such as the gain/phase imbalance in the quadrature modulator. The drawback of this approach is the large LUT size since the LUT needs to be two-dimensional and cover a large number of input levels.

Considering that the AM/AM and AM/PM responses of the memoryless power amplifier depend only on the input amplitude, the two-dimensional LUT in the mapping predistorter can actually be replaced by two one-dimensional LUTs. Indexed by the input amplitude $r_x(t)$, the one-dimensional LUTs specify the desired output amplitude, $A[r_x(t)]$, and the phase shift, $\phi_A[r_x(t)]$; i.e., the predistorted output is given by

$$z(t) = A[r_x(t)] e^{j\{\phi_x(t) + \phi_A[r_x(t)]\}}, \quad (6)$$

where $\phi_x(t)$ is the phase of the input signal $x(t)$. Since the predistortion LUTs are in polar form, this predistorter, proposed by Faulkner *et al.* [22], is often referred to as the polar structure predistorter. In practical implementations, phase calculation in the polar conversion for each input complex point is quite computationally intensive. Faulkner *et*